Extreme marine events revealed by lagoonal sedimentary records in Ghar el Melh during the last 2500 years in the northeast of Tunisia.

Balkis Samah Kohila[1, 2], Laurent Dezileau[2], Soumaya Boussetta[1], Tarek Melki[1], Nejib Kallel. [1]

5

[1] Laboratoire Géoressouces, Matériaux, Environnements et changements globaux, LR13ES23 (GEOGLOB), Faculté des Sciences de Sfax, BP1171, Sfax 3000, Université de Sfax, Tunisie.
[2] Laboratoire de Morphodynamique Continentale et Côtière (M2C), Université de Caen, UMR 6143, 14000 Caen, France.

10 *Correspondence to*: Balkis Samah Kohila (balkis.samah@yahoo.fr)

Abstract. The Tunisian coast has been affected in the past by many events of extreme marine submersion (storms and tsunamis). A high-resolution study along two sediment cores "GEM3" and "GEM4" taken from the lagoon of the Ghar el Melh was performed to identify the different paleo-extreme events and to reconstruct the paleo-environmental changes of the North-eastern part of Tunisia during the Late Holocene. A very high-resolution of analysis (sedimentological, granulometric, and geochemical) was applied on these cores. These cores were also dated with isotopic techniques (^{137}Cs, [210]Pbex, ^{14}C) and the outcomes reveal fives phases of paleoenvironmental changes of this lagoonal complex. The first phase dated from -275 to 200 Cal AD characterized by a high percentage of Silt and Clay (fine particles) indicating a protected lagoon. The second phase synchronous with the Dark Age Climatic Period dated from 300 to 1100 Cal AD, is marked by an increase in the coarse sediment and could be explained by a weakening of the sandy barrier due to an increase of storm events or/and the tsunami of 365 Cal AD. The third phase is characterized by a return to a closed lagoon during the Medieval Warm Period (from 1100 to 1690 Cal AD). The fourth phase dated from 1690 to 1760 Cal AD coincide with "the Little Ice Age" and is marked by one specific sedimentological layer attributed to a marine submersion event. This layer could be associated to the 1693 tsunami event in southern Italy or an increase of extreme storm events. The fifth phase covering the last 250 years present a reclosing of the lagoon.

25 **1 Introduction**

Coastal storms or tsunamis are among the most dangerous events that caused significant human and economic losses along coastal regions (Seisdedos et al., 2013). One of the strongest destructive and dangerous recorded meteorological event was that of the hurricane Katrina in Florida in United States in 2005. It engenders more than $100 billion of damages, killed around 2000 people and touched 90000 square miles of the United States (Phadke, 2005). The 2004 Sumatra tsunami was consecutive 30 to a mega-earthquake with $M_w9.2$. This tsunami has generated a high waves up to 30 meters and induced 250.000 dead peoples

(Lay et al., 2005). This tsunami was considered by many Indonesian peoples as the most disastrous event compared to other major past catastrophic events that had occurred in 1797 and 1833 (Natawidjaja et al., 2006).

The Mediterranean basin is defined as an "Hotspot" of the climate change (Lionello and Scarascia, 2018; Pausas and Millán, 2019). According to the IPCC (2014), the coastal erosion and submersion is one of the results of an elevation of sea-level due to the global warming. The Mediterranean Sea surface temperature has increased by almost 1°C since 1980 and expected to rise further by 2.5 °C in the next seventy years (Jacqueline Karas, 2006). In this context, the Mediterranean coastal zones will be probably more vulnerable to the climatic extreme events (storms and medicanes), and more exposed to coastal erosion processes and flooding (Seisdedos et al., 2013). The Mediterranean basin is also characterized by a high seismic activity due to its geographical position between the Eurasian and African plates (Papadopoulos and Fokaefs, 2005; Papadopoulos and Baskoutas, 2009). The earthquake of the 21st of May 2003 that happened in the Western Mediterranean Sub-basin precisely in Boumerdes (Algeria) with a magnitude of about 6.8 has generated a tsunami (Belazougui, 2008). The low wave generated has a height < 25cm and propagated from the Algerian coast toward the Murcia Province. These waves have not caused any evident damages (Álvarez-Gómez and Gonzalez, 2011). However, in the Eastern Mediterranean sub-basin, the Crete earthquake (21st July 365 AD) induced a tsunami that propagated across the region to reach Alexandria and has hit the Cretan coast causing extensive damage (François, 1984).

Due to the absence of data covering a sufficiently long time period, the recent instrumental data, and textual archive on extreme events (storm and tsunami) in Tunisia do not allow us to determinate any evolution in time. According to Morton et al.(2007); Dezileau et al.(2011); Sabatier et al.(2012) and Degeai et al.(2015), these sedimentary inputs coming from the sea during marine submersions, will permit the study of these extremes events over a longer period of time. A historical catalog of tsunamis and storms is being built in the Mediterranean region (e.g., Goldfinger et al., 2013), but there is a very few information on the Tunisian coasts. The aim of this study is to reconstruct the evolution of Ghar el Melh lagoon and to identify the different extreme events (storms or tsunamis) using a multi-proxy analysis based on geochemical and sedimentological approaches of two sediment cores GEM3 and GEM4 collected from the lagoon of the Ghar el Melh in the North-western part of the Gulf of Tunis.

2 The study site of Ghar El Melh

2.1 Geological Sitting

This work focuses on the Ghar el Melh lagoon situated in the Northeast of Tunisia. This lagoon is called also "the Porto Farina". It has an elliptic shape and approximately a surface of 28.5 km^2. Its average depth is about ~0.8 m (Romdhane, 1985; SCET-ERI, 2000; Moussa et al., 2005). This lagoon is directly limited in the north side by a mountain range called "Jbel Nadhour" (325 m). This mountain is composed of a marine Pliocene material (Figure 1) represented by sandstone sediments (Hamouda, 2014). The lagoon is bordered in the west and south side by recent quaternary marshy grounds formed by clay and

silt sediments. While in the eastern side, it is separated from the sea by a sandy barrier, with a local opening (El Boughaz) allowing a permanent hydraulic communication (Oueslati et al., 2006). This sandy barrier has formed by a littoral drift oriented from the North-East to the South-West (KHRYSTAL Engineering, 2003).

65   According to Paskoff (1994), the lagoon was considered as a vestigial and remaining part of the Utique Sea that was formed during the last postglacial transgression since 6000 years ago. Progressively, this small gulf has been disconnected from the Utique Sea, due to Medjerda fluvial deposits (Paskoff and Trousset, 1992). This caused a progressive reshaping of the lagoon to its present morphology, which could be attributed to an association of the shape of the coastline and alluvium deposition from the Medjerda River (Moussa et al., 2005). Over time, the delta of Medjerda was distinguished by a high flood peak and

70   a high interannual discharge variability. This river's average sediment yield is about 10 g/l and it is characterized by an annual average flow of 30 m3/s and reached 3500 m3/s in the exceptional flood of March 1973 where solid discharge is calculated around 100 g/l (Claude et al., 1977). A Large amounts of alluvium was carried by the Oued, estimated over 22 millions tonnes per year in the Gulf of Tunis before the construction of dams (Oueslati et al., 2006). The materials are deposited when the Oued reaches the low flood zones, contributing then to an extension of his delta towords the sea and a numerous changes of

75   channels (Delile et al., 2012).

In the Gulf of Tunis, the mean amplitude of semi-diurnal micro-tidal activities measures between 12 and 30 cm (El Arrim, 1996; Saïdi et al., 2012) The amplitude of the tidal range in this region was estimated around 35 cm (Oueslati, 1993). The coastal environment of the Gulf of Tunis was exposed to natural erosion processes provoked by waves, tides, and periodic storm-surges (Hzami et al., 2021). This erosion is the effect of the long shore coastal drift from the south-east to north-west

80   direction.

2.2 Climatological and hydrological settings

The Northeast of Tunisia is characterized by a typical Mediterranean climate with hot arid summer and rainy winter characterized generally by heavy rainfall periods and floods. The rainfall mean annual in the lower valley of the Medjerda is around 500 mm.yr^{-1} (Oueslati, 2004). Furthermore, in this study area, the rainfall rate is very variable. The mean winter

85   temperatures are around ~11 °C. The highest precipitation occurred mainly between November and December with an average of 248 mm (INS, 2001). The monthly average values sometimes exceed 100 mm (Beni Atta Station in December) and never fall below 60 mm (MEAT, 2001). The high temperatures are observed in August with mean values of ~27 °C. In other hand, the salinity in the lagoon depends on the hydrological balance and varies from 36 g/l in winter to 51 g/l in summer due to the highest evaporation rate (1450 mm/year) (Added, 2001; Moussa et al., 2005; Oueslati et al., 2006).

3 Material and methods

3.1 Sampling location and sediment samples

Two piston cores were manually collected in 2012 in the Northeast of Ghar el Melh lagoon. These cores are 126 cm (GEM4) and 98 cm (GEM3) in length and 10 cm in diameter (Figure 1). They were manually sampled according a transect East West into the lagoon (~200m from the sandy barrier for GEM3 and ~400m for GEM4). In the laboratory, the two cores GEM4 and GEM3 were divided, photographed, and described in detail. Before granulometric and geochemical analysis, the cores were split into 1 cm vertical sections. Moreover, 29 surface sediment samples of around 20 to 30g were collected from present-day soil horizons from the Medejerda watershed to the littoral area (beaches and dunes) to assess the origin and all sources of the lagoon sediment arriving in the study area: (i) 6 samples comes from the Medjerda River (Gr01 to Gr06), (ii) 12 samples from different small affluents located in the northern and western part of the lagoon (from Gr07 to Gr18) and (iii) 11 samples from the sandy barrier (Gr19 to Gr29) (Figure 1). For all samples, the position was registered using a GPS "GPS map 60, Garmin". In the laboratory, granulometric and geochemical analysis were performed on these surface samples. The particle sizes obtained are classified according to Folk and Ward (1957) into three categories (clay $\Phi < 2\mu m$, silt $2\mu m < \Phi < 63\mu m$ and sand $\Phi > 63\mu m$).

3.2 Sedimentology and geochemistry analysis

To determinate the distribution of grain size a particle Size analysis was adopted by using a Beckman Coulter© LS 13 320 (Geosciences Montpellier). Due to the high concentration of shells fragments (>200 µm), every sample was sieved at 150µm before analysis. An ultrasounds were used to avoid particles flocculation, after the entrance of sediments into the fluid module of the granulometric. We used an XRF core scanner Niton XL3t to analyzed sediment cores and surface samples by X-ray fluorescence (XRF). In order to avoid desiccation of the sediment and contamination of the XRF measurement unit, samples had to be covered with an Ultralean film. The geochemical analysis from XRF measurements was executed in the mining type ModCF proline mode. These semi-quantitative elemental measurements were performed along with the sediment core every 1 cm. The elemental concentrations obtained are expressed in ppm or percentage values. To evaluate the analytical error and the precision of measurement, international powder standards (NIST2702 and NIST2781) were adopted, it was between 10 and 25% for the Si, and lower than 5% for the Ca, Sr, Ti, Fe, Zn, Ba, and Rb, and between 5 and 10% for the Pb, Zr.

3.3 Chronological framework

To determinate the chronology of the two cores GEM4 and GEM3, an accelerator Mass Spectrometry (AMS) ^{14}C dates on only one mollusk species (*Cerastoderma glaucum*) associated with the using of ^{210}Pb and ^{137}Cs measurements were adopted. In fact, the ^{137}Cs and [210]Pbex activities analysis was measured by gamma spectrometry using a CANBERRA Broad Energy Ge (BEGe) detector on fine sediment (fraction < 150 µm). The [210]Pb$_{ex}$ dating is founded on the determination of the ^{210}Pb excess activities preserved in the sediment of cores. The utilize of this natural radionuclide ^{210}Pb to indicate sedimentation rate is

now a well-established technique (Goldberg, 1963; Krishnaswamy et al., 1971a; Robbins and Edgington, 1975). The dating of ^{137}Cs was released following the procedure of Robbins and Edgington (1975).

The ^{14}C analysis was conducted at the labratoire de Mesure C14 (LMC14) on the ARTEMIS accelerator in the French CEA institute (Atomic Energy Commission) at Saclay, France. These ^{14}C analyses were realized with the classical procedure
125 illustrated by Tisnérat-Laborde et al., 2001. The radiocarbon ages were transformed into calendar ages utilizing the Marine 13 curve (Reimer et al., 2009). The radiocarbon ages of marine and lagoonal organisms are generally older than the atmospheric 14C ages and have been calculated and modified by subtracting the « reservoir age » (Zoppi et al., 2001; Siani et al., 2001; Reimer and McCormac, 2002; Sabatier et al., 2010; Dezileau et al., 2016).

4 Results

130 ### 4.1 Characterization of different detrital surface sources

In coastal environments, the principal component analysis (PCA) was usually performed on the sediment sampled around lagoons in order to characterize the different sources of sediments deposited in the lagoon (Degeai et al., 2015; Gaceur et al., 2017; Affouri et al., 2017 and Khalfaoui et al., 2019) and to determine the several poles related to potential sediment sources supplies (Figure 2). We choose the Mn, Ti, Zn, Ba, Rb, Fe, Sr, Ca, and Si elements due to their good detection by the mobile
135 XRF. We established the calculation factors F1 61.12% and F2 11.13% of the geochemical dataset using the XLSTAT-2016 statistical software. The two first factorial factors represented in the PCA diagram present (Figure 2) 72.25% of the entire variance of the dataset. The factor 1 accounts for 61.12% of the entire variance. Factor number 1 is marked by a positive loading for terrigenous elements Rb, Ti, Ba, Mn, Fe, and Zn. Whereas the Ca and Sr present a modest positive loading and are inserted in factor 1. Factor 2 represents 11.13% of the global variance. It indicates positive loading for Si, Mn, Ti, Ba, Zn, Rb,
140 and Fe, whereas Sr and Ca have negative loadings. Based on these statistical analyses of geochemical data, three distinct sources of sediments were identified (Figure 2): (i) Terrigenous or Alluvial source (Mn, Fe, Zn, Ba, Rb) mainly discharged by rivers during floods. (ii) Marine source Si such as sands coming from the sandy barrier coastal during marine submersion; (iii) and a biogenic origin (Sr and Ca).

According to this funding, the sedimentation in the lagoon of the Ghar el Melh is generally manifested by marine and terrestrial
145 inputs. Indeed, the geographic distribution (Figure 3) of granulometric results indicates that the high percentage of coarse sediments "sands" (% >75%) are from the sandy barrier, whereas, sediments of the Medjerda watershed are distinguished by a very high percentage of fine sediments (Silt and Clay). Medjerda River and the affluent around it constitute the main origins of fine fractions (Clay) in the Ghar el Melh lagoon. The mapping of terrigenous elements such as Silicon, Titanium, and Iron contents in surface sediments confirm this distinction of detrital origins around the Ghar el Melh lagoon. High Si values
150 (>110000 ppm) distinguish especially the sandy barrier. Moreover, the highest contents of Titanium Ti (> 1400 ppm) and Iron Fe (> 17500 ppm) are retrieved in sediment from the watershed of the Medjerda (Figure 4). This difference in the origin of the

terrigenous inputs in Ghar el Melh lagoon could be explained by the fact that, during floods events, finer sediments are coming from the Medejerda watershed whereas, at the time of marine storms, coarse marine sand inputs are from the barrier.

Therefore, the geochemical analysis confirms the results of granulometric analysis by showing that the sedimentation of this lagoon was controlled by marine and continental contributions.

4.2 Downcore results

4.2.1 Age model

The chronology of the GEM3 and GEM4 cores has been established using the ^{14}C dates and also the^{137}Cs and ^{210}Pb measurements on monospecific mollusk shell samples and bulk sediments, respectively. In the uppermost 30 cm of the two cores, the measured ^{210}Pb$_{ex}$ values range in GEM3 from 287.47 to 2.29 mBqg^{-1} and f in GEM4 from 253.67 to 1.01 mBqg^{-1}. In general, the down-core distribution of ^{210}Pb excess values follows a relatively exponential decrease with depth. Based on a model Constant Flux, Constant Sedimentation Rate (CFCS) (applicated by Goldberg, 1963; Krishnaswamy et al., 1971), the ^{210}Pb data determinate a sedimentation rate of 0.7 mm year^{-1} for GEM3 and 0.6 mm year^{-1}for GEM4. The distribution profile of ^{137}Cs activity shows for the first 10 cm (Figure 5) a maximum value at 3.5 cm in GEM3 and 3 cm in GEM4. This can represent the period of the utmost radionuclide fallout in the Northern Hemisphere which was related to the weapons atomic peak testing in 1963. The ^{137}Cs obtained sedimentation rate is about ~0.7 mm year^{-1} for the GEM3 which is slightly higher than that obtained for GEM4 (0.6 mm year^{-1}; Figure 6). The distribution profile of the total Pb shows that the beginning of the industrial pollution in 1892 (Latour, 2019) is situated at 9 cm, indicating a sedimentation rate of about 0.75 mm year^{-1} for both cores (Figure 6). Thereby, sedimentation rate of the GEM3 core calculated using the ^{137}Cs, ^{210}Pb and total Pb show similar values around 0.75 mm year^{-1}, which are slightly higher than that for GEM4 (mean value of around of ~0.6 mm year^{-1}). The conventional AMS-^{14}C measurements were performed using mollusk shells (*Cerastoderma glaucum*) on eight control points for GEM3 (Table 1) and seven ones for the GEM4 (Table 2). Taking into account both the radiocarbon and^{210}Pb$_{ex}$ dates, the local ^{14}C reservoir age in the Ghar el Melh lagoon was determined. According to the method of Sabatier et al.(2010), the evaluation of the modern ^{14}C reservoir age was conducted by comparing an age obtained from ^{137}Cs and ^{210}Pb data, and from geochemical analysis of mining-contaminated lagoonal sediments with an AMS^{14}C age of a pre-bomb mollusk shell.

According to Reimer et al. (2013), the Sea surface reservoir age R(t) for the recent shell (SacA44506) was measured by subtracting the atmospheric ^{14}C value determined for the historical date 1845 AD (114±8 ^{14}C years) from the measured apparent ^{14}C ages of the shell (450±30 ^{14}C years, Table 3). This determines an R(t) value of 363 years. The deviance from the total mean reservoir age (ΔR) is then calculated by subtracting the marine age model value obtained for 1845 AD (488±23 ^{14}C years) from the measured apparent ^{14}C age of the mollusk (450±30 ^{14}C years; Table 3). The calculated ΔR around -38 years (Table 3) is thus, adopted. Finally, the age model of GEM3 and GEM4 cores was established by using the OxCal 4 on ^{14}C ages and ^{210}Pb$_{ex}$/^{137}Cs average sedimentation rates. The ^{14}C mean sedimentation rate calculated is then about ~2.5mm year^{-1} (Figure 7A).

As the GEM4 indicates a level of erosion or inactive deposition process named "a Condensed area" observed from 59 to 72
cm (between 0 and 1000 Cal AD/BC), which would instigate an error in the obtained age model (Figure 7B), the discussion
will be focused only on the ages estimated from GEM3 core. For the GEM4 core, the age correction has been obtained by the
correlation between the Strontium profile of the two cores GEM3 and GEM4.

4.2.2 Lithological, granulometric and geochemical studies of GEM3 and GEM4 cores

Two sedimentary cores were collected in the northeastern of Ghar el Melh lagoon. They contain fine sediments (clay and silt)
interbedded with coarse-grained layers formed by mollusk fragments and siliciclastic sand. The sedimentary succession in the
GEM3 core is very comparable to that presented in GEM4 (Figure 8). Whereas, the thickness of sandy layers is slightly
different between the two cores. This could be attributed to the geographical position of core GEM3, which is closer to the
sandy barrier (∼200m) than core GEM4 (∼400m).

The GEM3 and GEM4 sediment cores of 97 and 126 cm long show visual variation in the sediment composition. Lithological
description of these two cores highlighted three distinct sedimentary facies (Figure 8):

The Basal unit (1), situated between 126 - 67 cm in GEM4 and between 97 - 85 cm in GEM3, is composed generally of a
lighter grey silty layer and shells. At the base (the last 3 cm for the GEM3 and the last 13 cm for the GEM4) the lithological
composition of this unit is characterized by a very thin fine sandy layer. For the GEM3, the transition between unit (1) to unit
(2) is defined by a sharp contact.

The Middle Unit (2), situated between 85 -63 cm in GEM3 and between 66 – 60 cm in GEM4, is typically composed of a
lighter grey sandy layer with a combination of shell fragments and sands.

The Upper unit (3): <60 cm in GEM4 and <63 cm in GEM3, is composed mainly of organic-rich clay and shells with the
intercalation of a sandy layer with a discontinuity contact situated between 36 and 26 cm in GEM3 and between 30 and 24 cm
in GEM4 (Figure 8). This sand layer is usually characterized by coarse sediments with light colours and also dominated by
shell fragments. This coarse grain size layer intercalated in the mud sediments indicates an "energetic" event, relative to the
background sedimentation. It is probably linked to washover event and marine incursion during an intense event such as a
storm or tsunami.

The granulometric analysis shows that the silty clay is the most abundant fraction in our sediment cores (Figure 8). However,
sand is dominant at two levels. The first layer is observed between 86 and 64 cm in GEM3 and between 60 and 65 cm in
GEM4 whereas the second one is between 35 to 26 cm in GEM3 and from 30 to 24 cm in GEM4. These two layers are
characterized by the dominance of a sandy quartz material and shell fragments.

The geochemical analysis of GEM3 and GEM4 cores performed using an XRF core scanner, have detected 21 chemical
elements above the limit of detection. Among these elements, we choose to represent in Figure 8 only those with a significant
down core variation which are Si, Ca, Sr, and Ti. The Silicon will represent the marine geochemical pole, while Titanium

215   represents the terrigenous one. According to the granulometric and geochemical results of surface samples, the Ti is associated with the silt-clay fraction whereas the "Si" is associated with the sandy fraction. Furthermore, the highest Strontium Sr and Calcium Ca values in the two cores are found to be related with the silt-clay fraction between 62 and 33 cm in GEM3 and between 60 and 30 cm in GEM4. The Sr and Ca represent a biogenic geochemical pole linked to marine shells. These results are in agreement with those acquired by the statistical method (PCA) in surface samples.

5   Discussion

5.1 Site sensitivity to overwash deposits

The sensitivity of the site to the overwash deposits can result from several factors such as barrier elevation, sediment supply, inlet, and a change in sea level (Donnelly et al., 2004; Scileppi and Donnelly, 2007; Dezileau et al., 2016). Generally, an increase in sea level produces a moving of the barrier landward. Thus, the highest number of sand layers in a sediment core

225   can be the consequence of a simple sea-level change. In the Mediterranean Sea and especially during the last 5000 years, the sea level has stayed more or less stable (< 2 m, Pirazzoli, 1991; Lambeck and Bard, 2000). Studies concerning Holocene sea-level fluctuations along the Tunisian coast remain have suggested a stabilization in relative sea level during the last 6000 years (Jedoui et al., 1998), which is very small and probably not enough to completely change the deposition environment of the Ghar el Melh lagoon. Furthermore, sedimentation in the two cores commenced 2500 years ago, on this short period, the

230   influence of the seal-level change has not drastically affected sedimentation in the center of lagoon.

Cores GEM3 and GEM4 present generally a sedimentary sequence dominated by fine-grained sediments (clay and silt), suggesting that the lagoon of Ghar el Melh has succeeded in keeping a low-energy environment during the last 2500 years.

The proxies applied in this work (granulometry and geochemistry), as well as the sedimentary indicators (discontinuity contact), showed that all sandy coarse peaks present within the GEM3 and the GEM4 cores were deposited through marine

235   high-energy events and not by a gradual change in sea-level.

The presence of a nearby inlet may increase the sensitivity of a particular area to storm-induced deposition. It allows for storm energy to more easily penetrate into the back-barrier area, letting a lesser storm with lower wave surge transport coarse sediment into the back barrier. If a large inlet had existed over a long period and had provided a ready conduit for sand from the Gulf of Tunis to the Ghar el Melh lagoon, this would have been reflected in the cores (deposition of thick sand layer over

240   a long period of time). However, no evidence of such active tidal connection lasting a long time is found in sedimentological and geochemical data for the past 2500 years.

Granulometric and Geochemical observations on the GEM3 and the GEM4 cores show a sedimentary sequence dominated by silty-clay deposits and interrupted over time by some allochthonous coarse materials. To determinate the source of these sandy layers, we compared their geochemical attributes with those from surface samples. This allowed us to establish whether these

245   deposits had a continental (river floods) or marine origin (storms and tsunamis). The two sand deposits present in the GEM3 and GEM4 cores have a geochemical correlation with marine coastal surface samples; both show enrichment with Si and

8

depletion with Fe and Ti, which reveals a marine source for these high-energy deposits. The results demonstrate that Ghar el Melh lagoon has been confronted with different episodes of marine submersion during the last 2500 years.

5.2 Extreme events and paleoevironement changes

The Late Holocene lagoonal history of Ghar el Melh may be divided into five phases that record the connection between the lagoon and the sea in relation to the sandy barrier's evolution. The different phases can be described as follow:

The first phase, dated from -275 to 300 Cal AD, is marked by a high percentage of fine sediments (about 70 % of Silt) (Figure 9). Our geochemical results show a relatively high concentration of terrigenous elements Ti (around 250 ppm) and Fe (around 2500 ppm). This predominance of the fine fraction, rich in Ti and Fe, means that the lagoon is filled in sediments coming from the Medjerda River. The presence of fine material suggests that the hydrodynamic current in the lagoon is low, we have a protected lagoon with a sandy barrier well-constructed. This accumulation of fine sediment could also indicates a higher contribution of sediments from Medjerda River. Indeed, this interval (Roman Climatic Optimum)corresponds to a more humid phase in the North of Tunisia(Stevenson et al., 1993).

The second phase has started around 300 Cal AD and finished at 1100 Cal AD. Our granulometric and geochemical results demonstrate that the sedimentation of Ghar el Melh lagoon during this period was mainly controlled by a marine contribution. This phase is marked by a decrease in the percentage of silt, and a rise in the percentage of sand (about 80 %) and the presence of a discontinuity contact with the underlying unit. This time interval shows also the presence of a high amount of Silicon (Si >100000 ppm) (Figure 9) which stipulate an enhance in the sandy material supply. The decrease in the silty-clay fraction (10%) is can be related to a dilution by high marine inputs. The dominance of coarse sediment, rich in Si, could be explained by a weakening of the sandy barrier due to an increase of storm events. Degeai et al.(2015) and Sabatier et al.(2012) have clearly recorded a period of higher storm activity from 400 to 800 cal yr AD in the occidental part of the Mediterranean area. This period named Dark Age Cold Period coincides with the North Atlantic cooling phase known as Bond Event 1 (Bond et al., 2001). Dezileau et al.(2011) and Sabatier et al.(2012) have demonstrated that intervals of an enhance in storm activity in the Western Mediterranean area seem to be well related to the cold periods of the Holocene. During these cold periods, the sea ice was prolonged over the North Atlantic basin southward especially during winter (Lamb, 1995). Dezileau et al. (2011, 2016) hypothesized that this extends propose a rise in thermal gradient, leading to an enhanced lower tropospheric baroclinicity over a large Central European-Mediterranean domain. This mechanism related to a southward movement of storm track suggests an enhance of storm activity in the Western Mediterranean Sea, in accordance with simulation (Raible et al., 2007). This sand deposit may have had another origin. Indeed, this deposit was dated at around cal AD 332+/-30. This period coincides with the tsunami event of 365 AD. This extreme event was generated by an earthquake of 8.3 magnitudes and is supposed to have been the powerful ever in the regions of the Eastern Mediterranean. From a numerical modeling, Pararas-Carayannis and Mader, (2010) indicate that the 365 AD tsunami has heavily affected coastal areas throughout the Eastern Mediterranean region; Palestine, South Asia Minor, Cyprus, the Nile Delta, Careen, Apollonia. In the central part of the Mediterranean region

the cities of Eastern Sicily, the coastline of Calabria, and the islands of Aiolou have been affected (Pararas-Carayannis, 2011). In Tunisia, the recent archeological discovery of the immersed city of Neapolis in northern Golf of Hammamet in 2017 suggest the occurrence of a tsunami in 365 AD (Aounallah and Fantar, 2006; National Heritage Institute of Tunisia, 2017). We can thus hypothesize that our sand deposited around 365 cal AD could also be associated to this tsunami event.

The third phase, dated from 1100 to 1690 Cal AD, is marked by a decrease of sandy material and an increase of clay material (about 30%) (Figure 9). The concentration of terrigenous elements, Ti (around 400 ppm) and Fe (around 3500 ppm) (Figure 9) are high during this period. This kind of sedimentation is typically associated with the processes of decantation in the lagoon (Liu and Fearn, 2000; Donnelly et al., 2004). During this third phase, the lagoon is protected by a sandy barrier well-constructed. This increase in the silty-clay fraction could also be due to a decrease of storm activity and/or an increase of fine sediments transported into the lagoon by higher runoff of the Medjerda river during the Medieval Warm period.

The fourth phase has started at 1690 Cal AD and finished at 1760 Cal AD. This phase was characterized by a high deposition of sand, about 75 % of the total sediment (Figure 9), indicating an opening of the lagoon (Figure 10). This time interval was characterized by a sudden decrease of Sr (around 200 ppm) and Ca (around 55000 ppm) concentrations (Figure 9). The presence of coarse sediments can be explained by a higher marine influence. Interestingly, this coarse-grained layer is recorded in both cores (from 26 to 35 cm for GEM3 and from 24 to 30 cm for GEM4) collected at 200 m and 400 m from the sandy barrier respectively (Figure 10). Thus, this period could be a sign of an enhance of intense storm activity. Indeed, this interval corresponds to the historic period called "Little Ice Age" (LIA) which coincides with the North Atlantic cooling phase known as Bond Event 0 (Bond et al., 2001). Many studies (Sabatier et al., 2012; Degeai et al., 2015; Dezileau et al., 2016) have clearly recorded a higher storm activity between 1400 and 1800 cal yr AD in the occidental region of the Mediterranean Sea. This sand deposit could also be associated to a tsunami event. This period corresponds to the documented Sicilian tsunami that occurred in 1693 CE. Due to its geographic position, the Ghar el Melh lagoon may be affected by this 1693 tsunami.

The sedimentary characteristics of tsunamis or storms deposits are almost similar (Hawkes et al., 2007; Morton et al., 2007; Kortekaas and Dawson, 2007; Mamo et al., 2009). Regarding the diagnostic characteristics of storm or tsunami deposits, several studies have pointed out many hypotheses and determinate that their distinctions are very controversial (Tappin, 2007; Engel and Brückner, 2011; Sakuna-Schwartz et al., 2015). Considering the available data on GEM3 and GEM4 sediment cores, the hypothesis of tsunami or storm origin for this recorded extreme event remains open. Deciphering the origin of this event requires further investigations, such a modeling of tsunami wave propagation for example.

The fifth phase dated from 1760 to 2012 Cal AD, is characterized by fine sediments (Figure 9). This fifth phase shows a protected lagoon (Figure 10) and suggesting that no catastrophic intense sea events have struck Gar El Melh lagoon during this last phase.

6 Conclusion

To identify the paleo-extreme events (storms or tsunamis) and to reconstruct the paleo-evolution of the lagoon of the Ghar el Melh, in the Northeast of Tunisia, high resolution of sedimentological, geochemical and geochronological analysis were used. This approach gives information about the paleoenvironmental changes of Ghar el Melh lagoon and paleo-extreme events since 2300 years. Five phases have been identified: The first phase (from -275 to 300 Cal AD) indicates a protected lagoon. The second phase from 300 to 1100 Cal AD shows an opening lagoon and more marine inputs. This period was may be associated with a more storm activity during the Dark Age Cold Period but may also be related to the 356AD tsunami event. The third phase indicates an isolated lagoon and coincides with the Medieval Warm period (from 1100 to 1690 Cal AD). The fourth phase present an opening phase of the lagoon and may be due to an enhance of storm activity during the Little Ice Age dated or the occurrence of the 1693 tsunami event. The fifth phase covered the last 250 years and shows a reclosing lagoon. Even if our records allowed to detect past extreme events, it is not possible to differentiate if they are due to tsunamis or storms. Deciphering the origin of these events require further investigations.

Author contributions

All authors analyzed the results and prepared the manuscript.

References

Added, A.: Biogeochemical cycles of Org-C, Tot-N and Tot-S in the sediment of the Ghar El Melh Lagoon (north of Tunisia), J. Mar. Syst., 30(1), 139–154, 2001.

Affouri, A., Dezileau, L., Kallel, N., Affouri, A., Dezileau, L. and Kallel, N.: Extreme flood event reconstruction spanning the last century in the El Bibane Lagoon (southeastern Tunisia): a multi-proxy approach., Clim. Past, 18, 2017.

Álvarez-Gómez, J. A. and Gonzalez, M.: Tsunami hazard at the Western Mediterranean Spanish coast from seismic sources, Nat. Hazards Earth Syst. Sci., 11, 227–240, doi:10.5194/nhess-11-227-2011, 2011.

Aounallah, S. and Fantar, M.: À la découverte du Cap Bon, Guid. Hist. archéologique, Tunis, 2006.

El Arrim, A.: Etude d'impact de la dynamique sédimentaire e, Diplôme Dr. Spécialité en Géologie. Fac. des Sci. Tunis, 208p, 1996.

Belazougui, M.: Boumerdes Algeria Earthquake of May 21, 2003 : Damage Anaysis and behavior of Beam- Colum Reinforced

Concerte Structures, in The 14th World Conference on Earthquake Engineering October 12-17, 2008, Beijing, China, pp. 1–8., 2008.

345   Bond, G., Kromer, B., Beer, J., Muscheler, R., Evans, M. N., Showers, W., Hoffmann, S., Lotti-Bond, R., Hajdas, I. and Bonani, G.: Persistent solar influence on North Atlantic climate during the Holocene, Science (80-.)., 294(5549), 2130–2136, 2001.

Claude, J., Francillon, G. and Loyer, J.-Y.: Les alluvions déposées par l'Oued Medjerda lors de la crue exceptionnelle de mars 1973, Cah. ORSTOM, Hydrol, 11–14, 1977.

350   Degeai, J.-P., Devillers, B., Dezileau, L., Oueslati, H. and Bony, G.: Major storm periods and climate forcing in the Western Mediterranean during the Late Holocene, Quat. Sci. Rev., 129, 37–56, 2015a.

Degeai, J. P., Devillers, B., Dezileau, L., Oueslati, H. and Bony, G.: Major storm periods and climate forcing in the Western Mediterranean during the Late Holocene, Quat. Sci. Rev., 129, 37–56, doi:10.1016/j.quascirev.2015.10.009, 2015b.

Delile, H., Goiran, J.-P. and Bravard, J.-P.: CONTRIBUTION DU SIG A LA RECONSTITUTION DES PROCESSUS DE

355   PROGRADATION DE LA MAJERDA: quels enjeux pour le port d'Utique?, in Première Rencontre pour l'Etude du Quaternaire en Tunisie (Qt1)., 2012.

Dezileau, L., Sabatier, P., Blanchemanche, P., Joly, B., Swingedouw, D., Cassou, C., Castaings, J., Martinez, P. and Von Grafenstein, U.: Intense storm activity during the Little Ice Age on the French Mediterranean coast, Palaeogeogr. Palaeoclimatol. Palaeoecol., 299(1), 289–297, 2011.

360   Dezileau, L., Pérez--Ruzafa, A., Blanchemanche, P., Degeai, J. P., Raji, O., Martinez, P., Marcos, C. and Von Grafenstein, U.: Extreme storms during the last 6500 years from lagoonal sedimentary archives in the Mar Menor (SE Spain), Clim. Past, 12(6), 1389–1400, doi:10.5194/cp-12-1389-2016, 2016a.

Dezileau, L., Pérez-Ruzafa, A., Blanchemanche, P., Degeai, J.-P., Raji, O., Martinez, P., Marcos, C. and Grafenstein, U. Von: Extreme storms during the last 6500 years from lagoonal sedimentary archives in the Mar Menor (SE Spain), Clim. Past, 12(6),

365   1389–1400, 2016b.

Donnelly, J. P., Webb III, T., Murnane, R. and Liu, K.: Backbarrier sedimentary records of intense hurricane landfalls in the northeastern United States, Hurricanes Typhoons Past, Present. Futur., 55, 58–95, 2004.

Engel, M. and Brückner, H.: The identification of palaeo-tsunami deposits a major challenge in coastal sedimentary research, Coastline Reports, 17, 65–80, 2011.

370   Folk, R. L. and Ward, W. C.: Brazos River bar [Texas]; a study in the significance of grain size parameters, J. Sediment. Res., 27(1), 3–26, 1957.

François, J.: Le raz de marée du 21 juillet 365.[Du cataclysme local à la catastrophe cosmique], Mézanges l'Ecole française Rome. Antiq., 96(1), 423–461, 1984.

Gaceur, E., Desprat, S., Rouis-Zargouni, I., Hanquiez, V., Lebreton, V., Nebout, N. C. and Kallel, N.: Pollen distribution in

375   surface sediments of the northern Lower Medjerda valley (northeastern Tunisia), Rev. Palaeobot. Palynol., 247, 13–25, 2017.

Goldberg, E. D.: Geochronology with 210Pb, Radioact. dating, 121, 121–131, 1963.

Goldfinger, C., Morey, A. E., Black, B., Beeson, J., Nelson, C. H. and Patton, J.: Spatially limited mud turbidites on the Cascadia margin: Segmented earthquake ruptures?, Nat. Hazards Earth Syst. Sci., 13, 38, 2013.

Hamouda, S.: Etude de l'evolution de l'occupation et de l'utilisation du sol dans le delta de Mejerda par télédétection et SIG.,
380   2014.

Hawkes, A. D., Bird, M., Cowie, S., Grundy-Warr, C., Horton, B. P., Shau Hwai, A. T., Law, L., Macgregor, C., Nott, J., Ong, J. E., Rigg, J., Robinson, R., Tan-Mullins, M., Sa, T. T., Yasin, Z. and Aik, L. W.: Sediments deposited by the 2004 Indian Ocean Tsunami along the Malaysia-Thailand Peninsula, Mar. Geol., 242(1–3), 169–190, doi:10.1016/j.margeo.2007.02.017, 2007.

385   Hzami, A., Heggy, E., Amrouni, O., Mahé, G., Maanan, M. and Abdeljaouad, S.: Alarming coastal vulnerability of the deltaic and sandy beaches of North Africa, Sci. Rep., 11(1), 1–15, 2021.

INP (National Heritage Institute of Tunisia), 2017. Une ville antique decouverte au large des côtes tunisiennes: Neapolis. http://www.inp.rnrt.tn/index.php?option=com_allvideoshareandview=videoandslg=

INS: Annuaire statistique de la Tunisie., 2001.

390   IPCC: Climate Change 2014 Synthesis Report., 2014.

Jacqueline Karas: Climate Change and the Mediterranean Region., 2006.

Jedoui, Y., Kallel, N., Fontugne, M., Ismail, H. Ben, M'Rabet, A. and Montacer, M.: A high relative sea-level stand in the middle Holocene of southeastern Tunisia, Mar. Geol., 147(1–4), 123–130, 1998.

Khalfaoui, O., Dezileau, L., Degeai, J.-P. and Snoussi, M.: Reconstruction of past marine submersion events (storms and
395   tsunamis) on the North Atlantic coast of Morocco, Nat. Hazards Earth Syst. Sci. Discuss., (June), 1–14, doi:10.5194/nhess-2019-130-RC2, 2019.

KHRYSTAL Engineering: Zone Sensible Littorale de Sidi Ali El Mekki., 2003.

Kortekaas, S. and Dawson, A. G.: Distinguishing tsunami and storm deposits: an example from Martinhal, SW Portugal, Sediment. Geol., 200(3), 208–221, 2007.

400   Krishnaswamy, S., Lal, D., Martin, J. M. and Meybeck, M.: Geochronology of lake sediments, Earth Planet. Sci. Lett., 11(1–5), 407–414, 1971b.

Lamb, H. H.: Climate, History and the Modern World., 1995.

Lambeck, K. and Bard, E.: Sea-level change along the French Mediterranean coast for the past 30 000 years, Earth Planet. Sci. Lett., 175(3–4), 203–222, 2000.

405   Latour, E. de F. de: L'industrie minière en tunisie (1892-1937)., 2019.

Lay, T., Kanamori, H., Ammon, C. J., Nettles, M., Ward, S. N. and Aster, R.: The great Sumatra-Andaman earthquake of 26 December 2004, Science (80-.)., 88(1), 11–12, doi:10.1126/science.1118950, 2005.

Lionello, P. and Scarascia, L.: The relation between climate change in the Mediterranean region and global warming, Reg. Environ. Chang., 18(5), 1481–1493, 2018.

410   Liu, K. and Fearn, M. L.: Reconstruction of prehistoric landfall frequencies of catastrophic hurricanes in northwestern Florida

13

from lake sediment records, Quat. Res., 54(2), 238–245, 2000.

Mamo, B., Strotz, L. and Dominey-Howes, D.: Tsunami sediments and their foraminiferal assemblages, Earth-Science Rev., 96(4), 263–278, 2009.

MEAT: Communication Initiale de la Tunisie à la Convention Cadre des Nations Unies sur les changements climatiques., 2001.

415

Morton, R. A., Gelfenbaum, G. and Jaffe, B. E.: Physical criteria for distinguishing sandy tsunami and storm deposits using modern examples, Sediment. Geol., 200(3), 184–207, 2007.

Moussa, M., Baccar, L. and Ben Khemis, R.: La lagune de Ghar El Melh: Diagnostic écologique et perspectives d'aménagement hydraulique, Rev. des Sci. l'eau, 18, 13–26, 2005.

420

Natawidjaja, D. H., Sieh, K., Chlieh, M., Galetzka, J., Suwargadi, B. W., Cheng, H., Edwards, R. L., Avouac, J. P. and Ward, S. N.: Source parameters of the great Sumatran megathrust earthquakes of 1797 and 1833 inferred from coral microatolls, J. Geophys. Res. Solid Earth, 111(6), 1–37, doi:10.1029/2005JB004025, 2006.

Oueslati, A.: Les côtes de la Tunisie: géomorphologie et environnement et aptitudes à l'aménagement, Université de Tunis I., 1993.

425

Oueslati, A.: Littoral et aménagement en Tunisie: des enseignements de l'expérience du vingtième siècle et de l'approche géoarchéologique à l'enquête prospective, Publications de la Faculté des Sciences Humaines et Sociales., 2004.

Oueslati, W., Added, A. and Adeljaouad, S.: Acide Volatile Sulfides" et "simultaneously extracted metals dans les sédiments des carottes prélevées dans la lagune de Ghar El Melh, Nord Tunisien, Rev. Méditerr. Env., 1, 15–18, 2006.

Papadopoulos, G. A. and Baskoutas, I.: New tool for the spatio-temporal variation analysis of seismic parameters, Nat. Hazards Earth Syst. Sci., 9, 859–864, 2009.

430

Papadopoulos, G. A. and Fokaefs, A.: Strong tsunamis in the mediterranean sea : A re-evaluation, J. Earthq. Technol., 42(4), 159–170, 2005.

Pararas-Carayannis, G.: The earthquake and tsunami of July 21, 365 AD in the Eastern Mediterranean Sea-Review of Impact on the Ancient World-Assessment of recurrence and future impact., Sci. Tsunami Hazards, 30(4), 2011.

435

Pararas-Carayannis, G. and Mader, C. L.: The earthquake and tsunami of 365 AD in the eastern Mediterranean Sea, in Proceedings of the 9th US National and 10th Canadian Conference of Earthquake Engineering, vol. 25, p. 29., 2010.

Paskoff, R.: Le delta de la Medjerda (Tunisie) depuis l'Antiquité, Etud. Rurales, 15-29f Paskoff, R. and Trousset, P.: L'ancienne Baie d'Utique: du témoignage des textes à celui des images satellitaires, Mappemonde, 1, 30–34, 1992.

Pausas, J. G. and Millán, M. M.: Greening and Browning in a Climate Change Hotspot: The Mediterranean Basin, Bioscience, 69(2), 143–151, 2019.

440

Phadke, R.: Exposing Hurricane Katrina : The Scope of an Unnatural Disaster., 2005.

Pirazzoli, P. A.: World atlas of Holocene sea-level changes, Elsevier Oceanogr. Ser., 58, 1–280, 1991.

Raible, C. C., Yoshimori, M., Stocker, T. F. and Casty, C.: Extreme midlatitude cyclones and their implications for precipitation and wind speed extremes in simulations of the Maunder Minimum versus present day conditions, Clim. Dyn.,

445   28(4), 409–423, 2007.

Reimer, P. J. and McCormac, F. G.: Marine Radiocarbon Reservoir Corrections for the Mediterranean and Aegean Seas, Radiocarbon, 44(01), 159–166, 2002.

Reimer, P. J., Baillie, M. G. L., Bard, E., Bayliss, A., Beck, J. W., Blackwell, P. G., Ramsey, C. B., Buck, C. E., Burr, G. S., Edwards, R. L. and others: IntCal09 and Marine09 radiocarbon age calibration curves, 0--50,000 years cal BP, Radiocarbon,

450   51(04), 1111–1150, 2009.

Reimer, P. J., Bard, E., Bayliss, A., Beck, J. W., Blackwell, P. G., Bronk Ramsey, C., Buck, C. E., Cheng, H., Edwards, R. L., Friedrich, M., Grootes, P. M., Guilderson, T. P., Haflidason, H., Hajdas, I., Hatté, C., Heaton, T. J., Hoffmann, D. L., Hogg, A. G., Hughen, K. A., Kaiser, K. F., Kromer, B., Manning, S. W., Niu, M., Reimer, R. W., Richards, D. A., Scott, E. M., Southon, J. R., Staff, R. A., Turney, C. S. M. and van der Plicht, J.: IntCal13 and Marine13 Radiocarbon Age Calibration

455   Curves 0–50,000 Years cal BP, Radiocarbon, 55(4), 1869–1887, doi:10.2458/azu_js_rc.55.16947, 2013.

Robbins, J. A. and Edgington, D. N.: Determination of recent sedimentation rates in Lake Michigan using Pb-210 and Cs-137, Geochim. Cosmochim. Acta, 39(3), 285–304, 1975.

Romdhane, M. S.: Lagune de Ghar El Melh: milieu, peuplement, exploitation, Tunis (Tunisia)., 1985.

Sabatier, P., Dezileau, L., Blanchemanche, P., Siani, G., Condomines, M., Bentaleb, I. and Piquès, G.: Holocene variations of

460   radiocarbon reservoir ages in a Mediterranean lagoonal, Radiocarbon, 52(01), 91–102, 2010.

Sabatier, P., Dezileau, L., Colin, C., Briqueu, L., Bouchette, F., Martinez, P., Siani, G., Raynal, O. and Von Grafenstein, U.: 7000years of paleostorm activity in the NW Mediterranean Sea in response to Holocene climate events, Quat. Res., 77(1), 1–11, 2012.

Saïdi, H. B., Souissi, R. and Zargouni, F.: Impact of shore-parallel breakwaters on the microtidal coast of Hammam-Lif (North-

465   East of Tunisia), Arab. J. Geosci., 5(2), 345–352, 2012.

Sakuna-Schwartz, D., Feldens, P., Schwarzer, K., Khokiattiwong, S. and Stattegger, K.: Internal structure of event layers preserved on the Andaman Sea continental shelf, Thailand: tsunami vs. storm and flash-flood deposits, Nat. Hazards Earth Syst. Sci., 15(6), 1181–1199, 2015.

SAMAALI, H.: Etude de l'évolution de l'occupation et de l'utilisation du sol dans le delta de Mejerda par télédétection et

470   systèmes d'informations géographiques., Université de Sfax., 2011.

Scileppi, E. and Donnelly, J. P.: Sedimentary evidence of hurricane strikes in western Long Island, New York, Geochemistry, Geophys. Geosystems, 8(6), 2007.

Seisdedos, J., Mulas, J., González de Vallejo, L. I., Rodríguez Franco, J. A., Gracia, F. J., del Río, L. and Garrote, J.: Estudio y cartografia de los peligros naturales costeros de la region de Murcia, Bol. Geol. y Min., 124(3), 505–520, 2013.

475   Siani, G., Paterne, M., Michel, E., Sulpizio, R., Sbrana, A., Arnold, M. and Haddad, G.: Mediterranean Sea surface radiocarbon reservoir age changes since the last glacial maximum, Science (80-.)., 294(5548), 1917–1920, 2001.

Stevenson, A. C., Phethean, S. J. and Robinson, J. E.: The palaeosalinity and vegetational history of Garaet el Ichkeul, northwest Tunisia, The Holocene, 3(3), 201–210, 1993.

Tappin, D. R.: Sedimentary features of tsunami deposits—Their origin, recognition and discrimination: An introduction, 2007.

480   Tisnérat-Laborde, N., Poupeau, J. J., Tannau, J. F. and Paterne, M.: Development of a semi-automated system for routine preparation of carbonate samples, Radiocarbon, 43(2A), 299–304, 2001.

Zoppi, U., Albani, A., Ammerman, A. J., Hua, Q., Lawson, E. M. and Barbero, R. S.: Preliminary estimate of the reservoir age in the lagoon of Venice, Radiocarbon, 43(2A), 489–494, 2001.

485

16
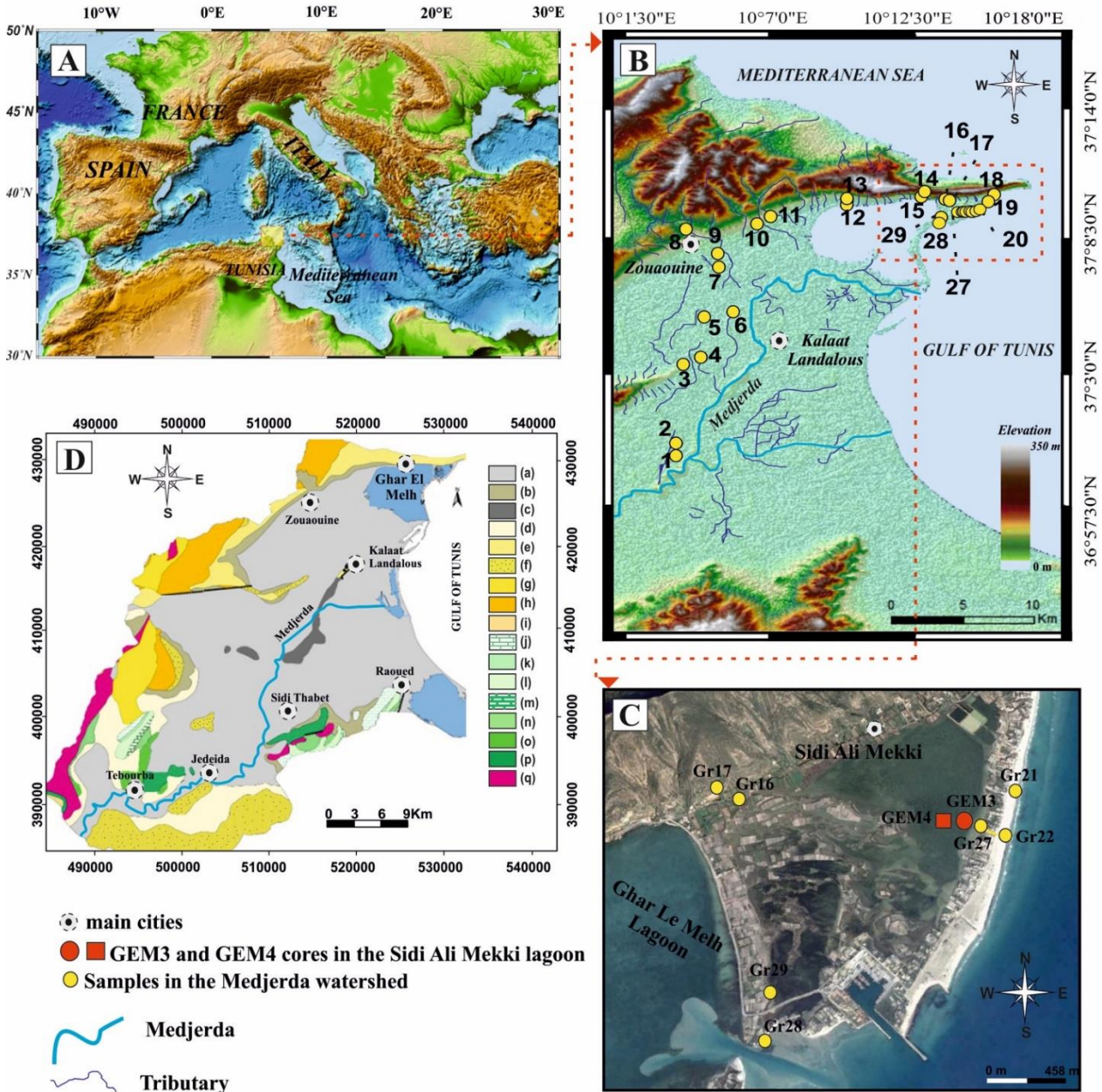
Figure 1: Maps of geographic setting of the Ghar el Melh Lagoon. (A) Position of the studied region in the Northeastern Mediterranean (Ocean Data View 2013). (B)Topographic map of the lagoon and the emplacement of the different surface sediment samples preleved from the coastal plain of the Medjerda (Created by Radewane Hout using Arcgis). (C) Topographic map of the Ghar el Melh lagoon and its surroundings (e.g ©Google Earth). (D) Geological maps of the Medjerda watershed (*(a) Recent alluvial soils (b) Slope deposits (c) Marine Quaternary (d) Villafranchienen (e) Pliocene (f) Continental Pliocene (g) Upper Miocene (h) Flyche de Kchabta (i) Lower Eocene (j) Maastrichtian (k) Senonian (l) Cenomanian (m) Albian (n) Aptian (o) Barrenian (p) Valanginian-Hautrevian (q) Triassi))*** (Geological Map; Paper n ° II of Bizerte at 1/200000 modified from Samaali Hamouda, 2011).**

490
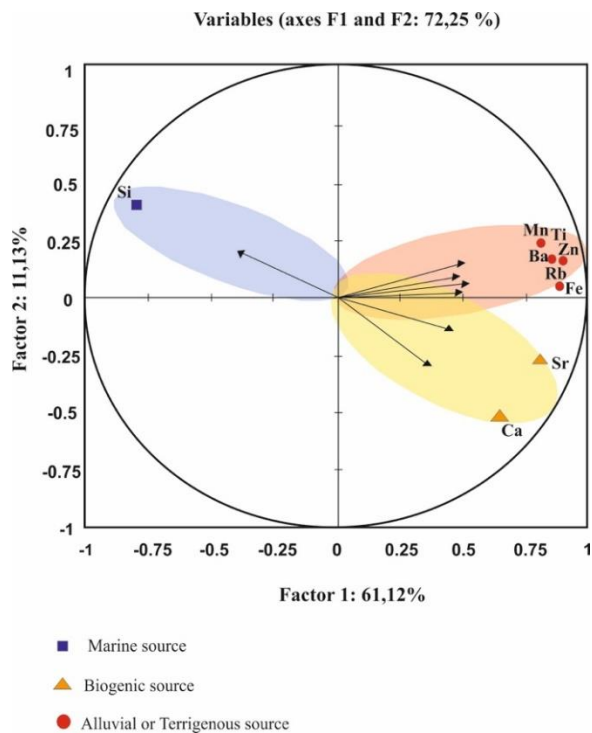
Figure 2: The different surface sediment sources from the Medjerda watershed and Ghar el Melh lagoon obtained by using a statistic model "A Principal component analysis" (PCA).
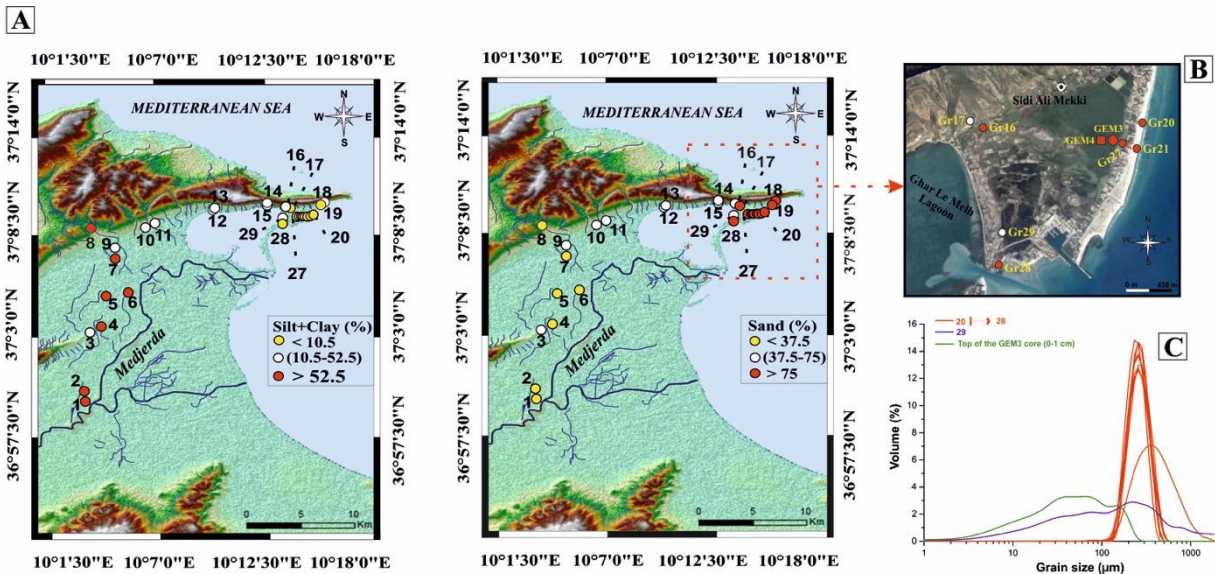
495

Figure 3: (3A): Topographic maps of the sand, Silt, and Clay percentage distributed in the Medjerda watershed and around the lagoon of the Ghar el Melh (Created by Radewane Hout using Arcgis). (3B) Topographic map of the two cores and the different sediment samples collected from Ghar el Melh lagoon and its surroundings (e.g © Google Earth). (3C): Particle size distributions (φ < 2000 µm) of representative samples around the Ghar el Melh lagoon.
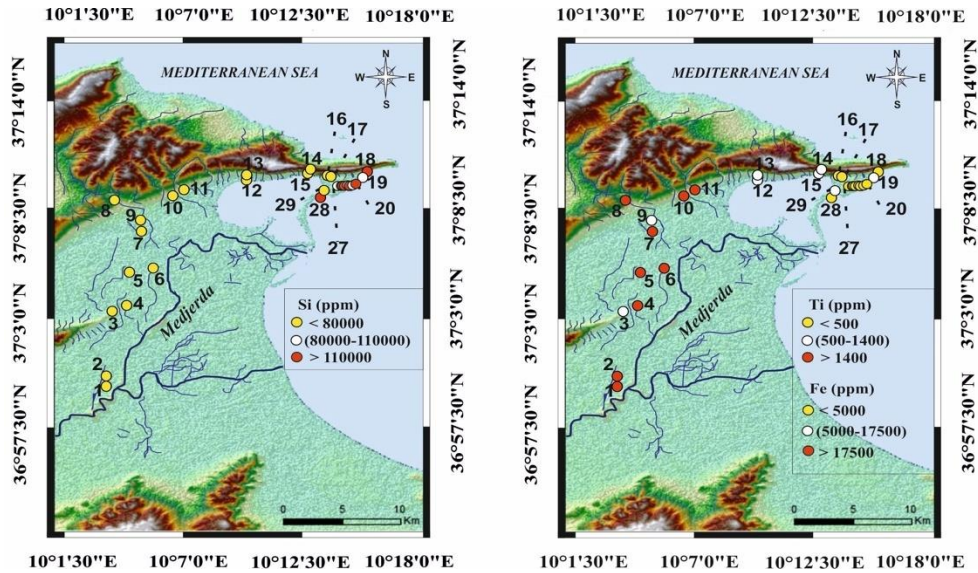

Figure 4: Topographic maps of the Iron (Fe), Titanium (Ti) and Silicon (Si) contents in the coastal plain of Medjerda and around Ghar el Melh lagoon (Created by Radewane Hout using Arcgis).

18
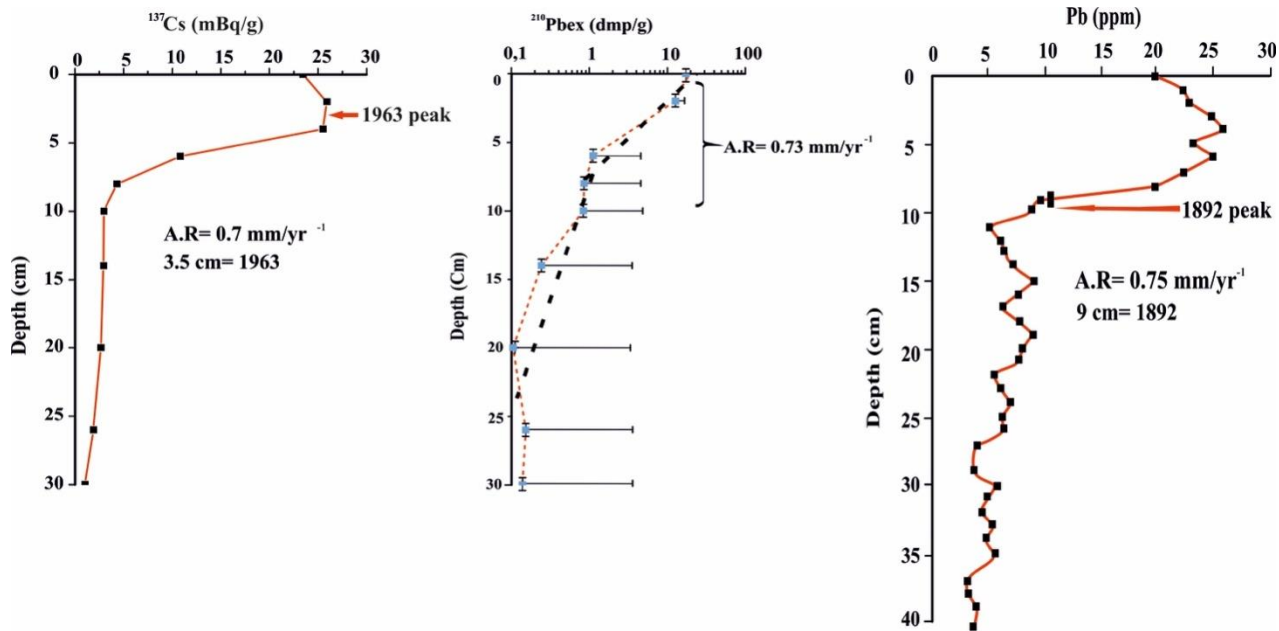
Figure 5: Distributions profile of ^{210}Pbex, Pb and ^{137}Cs vs. depth in the GEM3. The ^{210}Pb data determinate a sedimentation rate of 0.73 mm year^{-1}. The activity depth profile Cs present a peak at 3.5 cm, indicating in accumulation rates of 0.7 mm year^{-1} for the 1963 depths.
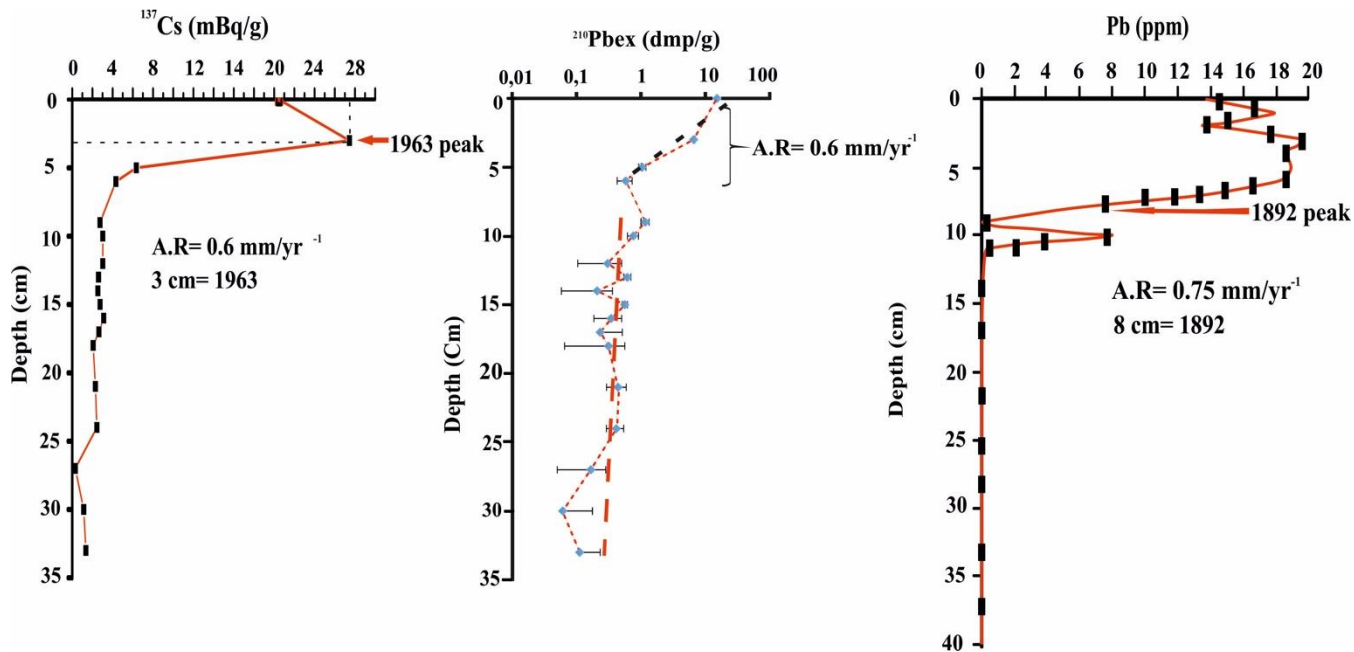
515   **Figure 6: Distributions profile of ^{210}Pbex, Pb and ^{137}Cs vs. depth in the GEM4. The ^{210}Pb data present a sedimentation rate of 0.6 mm year-1. The activity depth profile Cs indicate a peak at 3 cm, determining in accumulation rates of 0.6 mm year^{-1} for the 1963 depths.**
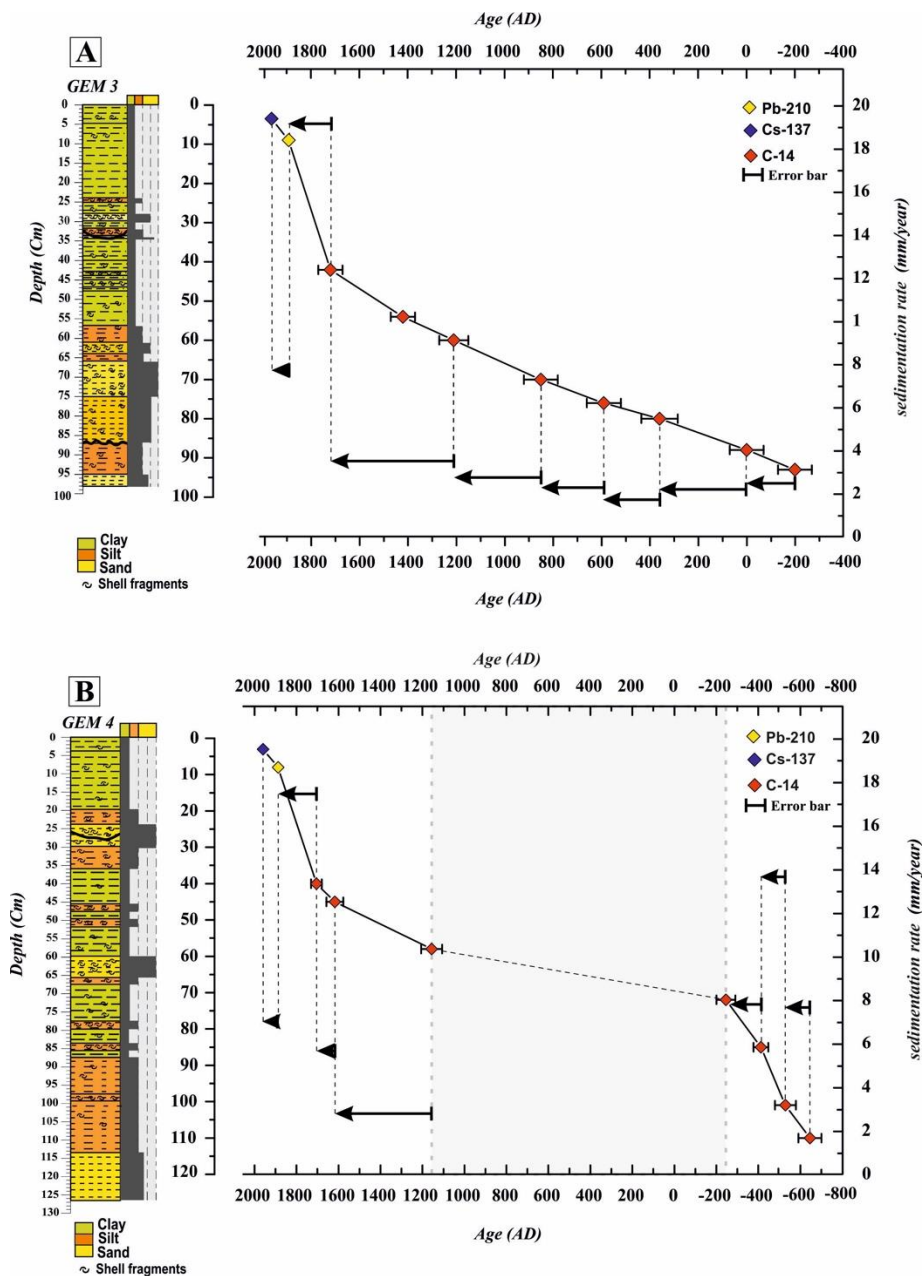
Figure 7: (7A): Sediment age-depth for the core GEM3 sampled from Ghar el Melh lagoon (Arrows: sedimentation rates variation).
520 **The OxCal 4.3 have been used to calculated the age model with 8 samples for ^{14}C dates and only one sample for each Pb and Cs dates. (7B): Sediment age-depth for the core GEM3 sampled from Ghar el Melh lagoon (Arrows: sedimentation rates variation). The OxCal 4.3 have been used to calculated the age model with 7 samples for ^{14}C dates and only one sample for each Pb and Cs dates. The blue band determines a period of inactive deposition process or erosion so-called "a Condensed area".**

20
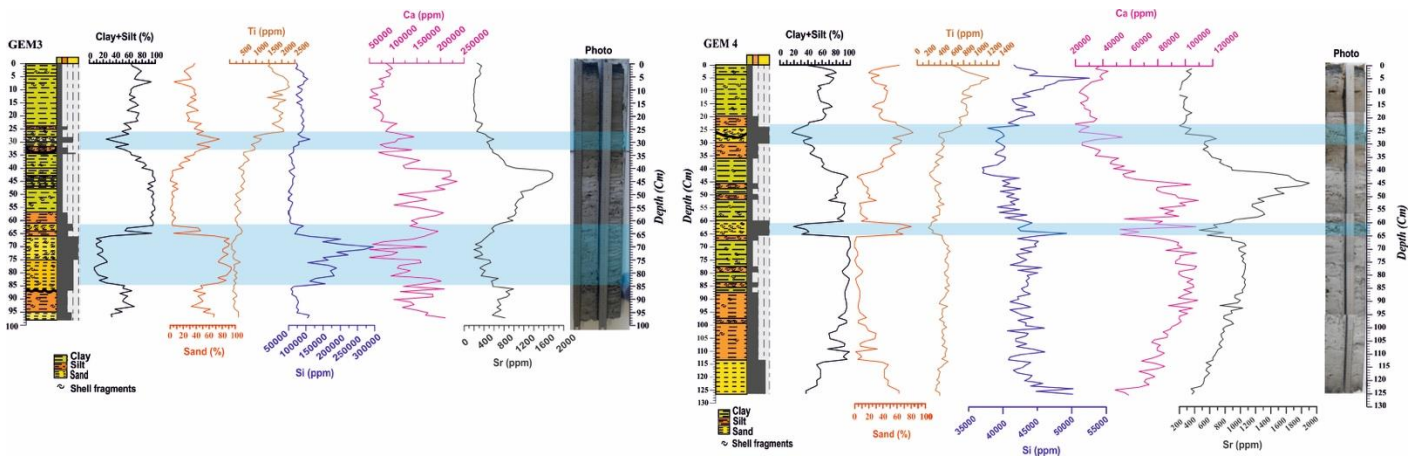
525

Figure 8: Stratigraphic log and grain size results of GEM3 and GEM4 cores compared to the results obtained from the XRF records (Titanium, Silicon, Calcium and Strontium) distributing in the two cores, vs. depth.
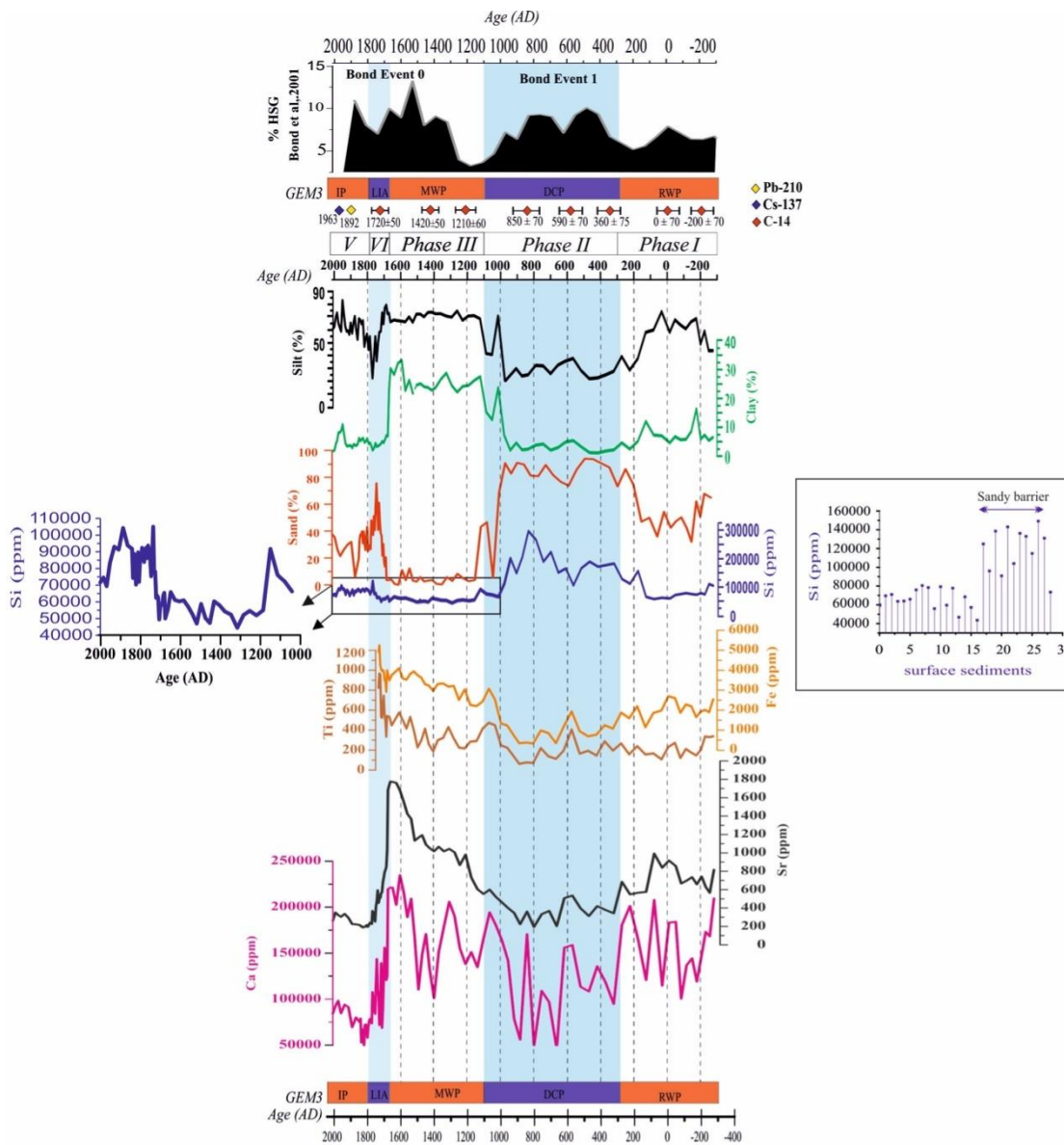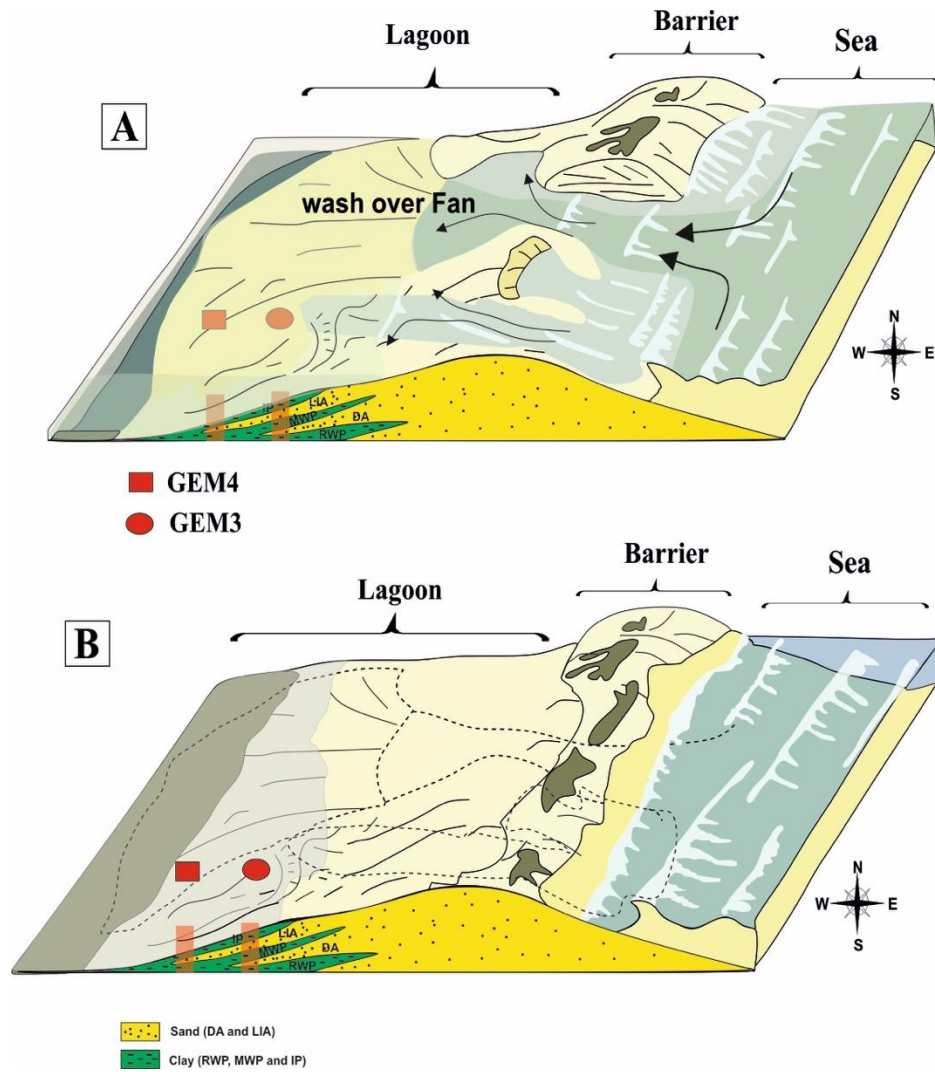
530

535

Figure 9: Evolution of grain size population compared to the results obtained from the XRF records (Iron, Calcium, Silicon, Titanium and Strontium) distributing in the GEM3 core, vs. age from -275 till 2012 AD. The two blue bands indicate a period of the Lagoon opening.

540

545

Figure 10: 3D diagram of the lagoon Ghar el Melh evolution. (A) Opening of the sandy lido and deposition of the washover in the lagoonal sediment. (B) Reclosure of the lagoon.

550

555

Tables

Tab.1. **¹⁴C data for shells from GEM3. The model ages were determined by the Oxcal. The ¹⁴C ages are calculated and calibrated using the curve of Marine 13 calibration with reservoir age.**

Labo code	Mollusk used	Depth (cm)	δ¹³C (‰)	¹⁴C ages (BP)	¹⁴C ages (Cal AD) (One Sigma ranges) [Start: end]
SacA 42679	*Cerastoderma glaucum*	42	-0.8	565±30	[cal AD 1692: cal AD 1765]
SacA 42685	*Cerastoderma glaucum*	54	1.5	930±30	[cal AD 1399: cal AD 1451]
SacA 42683	*Cerastoderma glaucum*	60	0.2	1195±3	[cal AD 1186: cal1260]
SacA 42681	*Cerastoderma glaucum*	70	0.2	1535±30	[cal AD 811: cal AD 902]
SacA 42680	*Cerastoderma glaucum*	76	1.4	1830±30	[cal AD 550: cal AD 630]
SacA 42686	*Cerastoderma glaucum*	80	0.6	2015±30	[cal AD 332: cal AD 424]
SacA 42684	*Cerastoderma glaucum*	88	-1.1	2350±30	[cal BC 67: cal AD 33]
SacA 42682	*Cerastoderma glaucum*	93	-1.4	2490±30	[cal BC 267: cal BC 144]

560

Tab.2. **¹⁴C data for shells from GEM4. The model ages were determined by the Oxcal. The ¹⁴C ages are calculated and calibrated using the curve of Marine 13 calibration with reservoir age.**

Labo code	Mollusk used	Depth (cm)	δ¹³C (‰)	¹⁴C ages (BP)	¹⁴C ages (Cal AD) (One Sigma ranges) [Start: end]
SacA42676	*Cerastoderma glaucum*	40	-3.7	490±30	[cal AD 1807: cal AD 1906]
SacA42675	*Cerastoderma glaucum*	45	1.8	615±30	[cal AD 1652: cal AD 1712]
SacA42673	*Cerastoderma glaucum*	55	0.3	1181±30	[cal AD 786: cal AD 1344]
SacA42672	*Cerastoderma glaucum*	72	-2.9	2545±30	[cal BC 332: cal BC 225]
SacA42674	*Cerastoderma glaucum*	85	-4.3	2660±30	[cal BC 431: cal BC 353]
SacA42678	*Cerastoderma glaucum*	101	-6.6	2625±30	[cal BC 399: cal BC 339][a]
SacA42677	*Cerastoderma glaucum*	110	-4.8	2725±30	[cal BC 512: cal BC 400]

[a]Age inversion

565

570 **Tab.3 .^{14}C age of recent pre-bomb mollusk samples in GEM4 core. The reservoir age R(t) and ΔR were calculated using the ^{210}Pbex date**

Labo code	^{210}Pb age (AD)	^{14}C year (BP)	Tree-ring ^{14}C age (BP) IntCall 13	Reservoir age R(t) (year)	Model age (Marine 4 curve)	Δ R (year)
SacA44506	1845	450±30	114±8	336	488±23	-38